Journal of Molecular Catalysis A: Chemical 315 (2010) 86–98

Contents lists available at ScienceDirect

Journal of Molecular Catalysis A: Chemical

journal homepage: www.elsevier.com/locate/molcata

Ethylbenzene to chemicals: Catalytic conversion of ethylbenzene into styrene over metal-containing MCM-41

Andressa H. de Morais Batista[a,1], Francisco F. de Sousa[b,2], Sara B. Honorato[b,2], Alejandro P. Ayala[b,2], Josue M. Filho[b,2], Francisco W. de Sousa[a,1], Antonio N. Pinheiro[a,1], J.C.S. de Araujo[a,1], Ronaldo F. Nascimento[a,1], Antoninho Valentini[a,1], Alcineia C. Oliveira[a,*]

[a] Universidade Federal do Ceará, Campus do Pici-Bloco 940, Langmur Lab. de Adsorção e Catálise, 60000000, Fortaleza, Ceará, Brazil
[b] Universidade Federal do Ceará, Campus do Pici-Bloco 922, Departamento de Física, Fortaleza, Ceará, Brazil

ARTICLE INFO

Article history:
Received 20 March 2009
Received in revised form
14 September 2009
Accepted 15 September 2009
Available online 18 September 2009

Keywords:
MCM-41
Metals
Ethylbenzene
Deactivation
CO_2

ABSTRACT

Isomorphously substituted (MeDM) and impregnated metal-containing MCM-41 (MeO_x/IM) catalysts, in which Me = Co, Cu, Cr, Fe or Ni, have been prepared. Structural and textural characterizations of the catalysts were performed by means of X-ray diffraction (XRD), chemical analysis, Raman spectroscopy, electron paramagnetic resonance (EPR), N_2 adsorption isotherms and temperature programmed reduction (TPR). Cu^{2+}, Co^{2+}, and Cr^{4+}/Cr^{3+} species were found over the catalysts as cations incorporated in the MCM-41 structure (MeDM) or highly dispersed oxides on the surface (MeO_x/IM). The MeDM catalysts exhibited a good performance in the dehydrogenation of ethylbenzene with CO_2. However, MeO_x/IM catalysts had a low performance in styrene production (activity less than 15×10^{-3} mmol h^{-1} and selectivity for styrene less than 80%) due to the high reducibility of the metals species. However, Ni^{2+} or Fe^{3+} coordinated with the MCM-41 framework, as well as NiO_x and Fe_2O_3 extra-framework species, is continuously oxidized by the CO_2 to maintain the active sites for dehydrogenating ethylbenzene. Deactivation studies on the FeDM sample showed that Fe^{3+} species produced active sp^2 carbon compounds, which are removed by CO_2; the referred sample is catalytically selective for styrene and stable over 24 h of reaction. In contrast, highly active Ni^{2+} and Ni^0 species produced a large amount of polyaromatic carbonaceous deposits from styrene, as identified by TPO, TG and Raman spectroscopy. An acid–base mechanism is proposed to operate to adsorb ethylbenzene and abstract the β-hydrogen. CO_2 plays a role in furnishing the lattice oxygen to maintain the Fe^{3+} active sites in the dehydrogenation of ethylbenzene to form styrene.
© 2009 Elsevier B.V. All rights reserved.

1. Introduction

Due to the increasing demand for energy-saving processes, the exploration of alternative technologies as a source of chemical production is under way worldwide. The dehydrogenation of ethylbenzene with CO_2 to produce styrene, for instance, is an important example of the application of a more ecological and economical process [1–8].

Currently, styrene monomer is used in the petrochemical industry to produce valuable commodities, including expandable styrene-butadiene latex, acrylonitrile–butadiene–styrene resins and a variety of polymers [9–11]. The overall reaction of styrene production by the dehydrogenation of ethylbenzene in the presence of CO_2 is given as reaction (I) [4,5]:

$$C_6H_5CH_2{-}CH_3 + CO_2 \rightarrow C_6H_5CH{=}CH_2 + CO + H_2O \quad (I)$$

Other possibilities to obtain styrene are: the catalytic dehydrogenation of ethylbenzene in the presence of steam (reaction (II)); the dehydrogenation of ethylbenzene using oxygen over carbon-based catalysts (reaction (III)); as a byproduct in the epoxidation of propene with ethylbenzene hydroperoxide over Mo-complex-based catalysts.

$$C_6H_5CH_2{-}CH_3 \rightarrow H_2 + C_6H_5CH{=}CH_2 \quad \Delta H_{298\,K} = 28.1\ \text{kcal mol}^{-1} \quad (II)$$

$$C_6H_5CH_2{-}CH_3 + 0.5O_2 \rightarrow C_6H_5CH{=}CH_2 + H_2O$$
$$\Delta H_{298\,K} = -29.7\ \text{kcal mol}^{-1} \quad (III)$$

The catalytic dehydrogenation of ethylbenzene with steam is usually performed over iron oxide, which is generally highly promoted by metals (Styromax Process) and accounts for more than 90% of

* Corresponding author. Tel.: +55 85 33 66 90 41; fax: +55 85 33 66 99 82.
E-mail address: alcineia@ufc.br (A.C. Oliveira).
[1] Tel.: +55 85 33 66 90 41; fax: +55 85 33 66 99 82.
[2] Tel.: +55 85 33 66 90 08; fax: +55 85 33 66 90 08.

1381-1169/$ – see front matter © 2009 Elsevier B.V. All rights reserved.
doi:10.1016/j.molcata.2009.09.006

the 25 million tons of styrene monomer produced by the industry annually [11–14]. However, processes that use oxygen and epoxidation of propene do not efficiently convert ethylbenzene to styrene.

The steam-based process (reaction (II)) has a significant thermodynamic limitation for ethylbenzene conversion, because it uses large amounts of overheated steam and the catalyst deactivation is irreversible [15,16]. Therefore, the steam process is a penalizing process in energetic costs for the industry [17]. However, the process that uses oxygen (reaction (III)) is free from thermodynamic constraints regarding conversion and operates at lower temperatures, since it is an exothermic reaction. The potentially oxygen-containing mixture and the deep oxidation of styrene to carbon oxides are the main drawbacks of this process [17–20]. In contrast, reaction (I) is a well-known and widely applied technique by researchers that focus on more environmentally friendly alternatives to produce styrene, which avoids the vaporization of tons of water, and thus, less energy is needed.

Therefore, the dehydrogenation of ethylbenzene using CO_2 instead of steam appears to be a better method since carbon dioxide, which is one of the major greenhouse gases, prevents hotspots on the catalyst surface, accelerates the reaction and avoids a chemical equilibrium [1–11,15]. However, the dehydrogenation of ethylbenzene with CO_2 is still only performed on a laboratory scale because of lack of active and stable catalyst systems. Indeed, since Fe catalysts promoted by potassium (10%) and other components (Al_2O_3, Cr_2O_3, Pd, Co, V, Ce, W and Mo) [18–20] used for commercial dehydrogenation process with steam do not work efficiently in the presence of CO_2, this has motivated the evaluation of carbon dioxide on new catalysts systems.

It is well known that the dehydrogenation of ethylbenzene in the presence of CO_2 can be performed with good styrene selectivity using a variety of catalysts [1–13]. Additionally, supported catalysts containing only non-precious metals, e.g., nickel, iron, cobalt, chromium, lanthanum, copper and vanadium, were successfully applied and performed comparably to the precious metal catalysts [8–20].

Among the catalysts studied, the molecular sieve-supported oxide catalysts were found to be the most promising in the dehydrogenation of ethylbenzene with carbon dioxide due to their high catalytic activity [19–22]. Thus, mesoporous molecular sieves, such as MCM-41, HMS, SBA-15, and silicalite mesoporous zeolite with highly ordered mesoporous channels and a controllable pore size (ca. 2–10 nm) and a high surface area, have been screened in the reaction with the MCM-41-based catalyst being superior to their analogues in terms of stability [18,21]. Also, similar catalytic behavior has been observed in the case of the direct thermal synthesis of Me-MCM-41 (where Me = Cr, Ga, Ni, V, Mn, Fe, or Co) for catalytic reactions, such as the dehydrogenation of propane with CO_2 [23], oxidation of alkyl hydroperoxides [22,23] and the dehydrogenation of ethylbenzene with CO_2 [18].

The direct-hydrothermally synthesized Me-MCM-41 mesoporous molecular sieves have been shown to have high catalytic performance due to factors such as: enhancement in redox and acid–base properties of the systems, relatively high thermal stability and textural properties (e.g., their high surface area and uniform pore size) that avoid coke formation [18,23]. Although limited studies on the oxidative dehydrogenation of ethylbenzene with CO_2 with mesoporous materials exist, a detailed investigation of materials, i.e., Me-MCM-41 or MO_x/MCM-41, for the new dehydrogenation process has not yet been carried out.

For a deep understanding and improvement of styrene production using the dehydrogenation of ethylbenzene with CO_2, the effect of two different preparation methods on the catalytic performance was studied in the present contribution.

The isomorphous substitution method has a tendency to incorporate metals inside the framework of MCM-41, while supporting the metals on the solid by impregnation provides highly dispersed locations of the metals on the wall surfaces inside the mesopores [24,25]. That is to say, through the modification of MCM-41 by incorporating M^{n+} ions into the porous framework or by depositing MO_x onto the surface, one can manipulate the physicochemical properties of both Me-MCM-41 and MO_x/MCM-41. This strongly suggests that the influence of the preparation method must be discussed in detail to explain which type of metal species act in the dehydrogenation of ethylbenzene with CO_2. This was achieved by characterization of the physicochemical properties of the catalysts by XRD, N_2 isotherms adsorption, TPR, chemical analyses, Raman spectroscopy, TG/DSC, and EPR, as well as the catalytic performance in dehydrogenating ethylbenzene using CO_2 as a mild oxidant.

2. Experimental

2.1. Catalyst preparation

The MCM-41 mesoporous silica was synthesized by adopting the procedure reported by Grün et al. [26]. In a standard method of synthesis, 0.81 g of cetyltrimethylammonium bromide (CTAB, Reagen) was dissolved in 17.7 mL of water under vigorous stirring at 70 °C for 10 min. After cooling this solution, a mixture of 10.3 mL of ethanol (99%, Vetec) and 8.1 mL of ammonium hydroxide was added and the solution was stirred for an additional 10 min. Then, 15 g of tetraethyl orthosilicate (TEOS, Aldrich 98%) was added dropwise to the solution with stirring for an additional 24 h. The molar composition of the resultant mixture was 1 TEOS:0.3 CTAB:11 NH_3:144 H_2O:58 EtOH.

After being stirred continuously, the precipitate was filtered, washed with deionized water, acetone, and dried at 60 °C for 4 h. The solid product was finally heated to 550 °C at a ramp rate of 1 °C min^{-1} in an air flow and calcined at this temperature for 5 h to give purely siliceous MCM-41, denoted as M.

A series of catalysts was prepared by isomorphous substitution using the so-called direct method (DM) by following a method similar to that described above using aqueous solutions of the metal salts: iron nitrate ($Fe(NO_3)_3{\cdot}9H_2O$, Reagen), nickel nitrate ($Ni(NO_3)_2{\cdot}6H_2O$, Reagen), cobalt nitrate ($Co(NO_3)_2{\cdot}6H_2O$, Vetec), copper nitrate ($Cu(NO_3)_2{\cdot}3H_2O$, Reagen) and chromium acetate (CrAc, Vetec).

It is important to point out that metal solutions were the last reactant added to the synthesis. The obtained catalysts were denoted as MeDM, where Me corresponds to Cr, Co, Fe, Cu or Ni, and DM represents MCM-41 prepared by the isomorphous substitution method. The percentage of metals was approximately 1 wt% hereafter.

Another series of catalysts was prepared by adopting the incipient wetness impregnation approach (IM). Aqueous solutions of the aforementioned precursors with 1 wt% of metals were added separately to 1 g of the pure MCM-41 support under stirring. The catalysts were marked as follows: the denotation of MeO_x/IM contains the abbreviation of the Cr, Co, Fe, Cu or Ni, and it indicates each metal loaded, while IM represents the MCM-41 support.

2.2. Characterization of catalysts

Both MeDM and MeO_x/IM catalysts were characterized by various techniques.

Inductively coupled plasma (ICP) optical emission spectroscopy was used to measure the concentration of nickel, copper, iron, chromium and nickel in each of the samples synthesized above. A 0.1 g sample of the catalysts was dissolved in 40 wt% hydrofluo-

ric acid solution and heated at 200 °C in a sand bath. The solution obtained was evaporated and dried, and a solution of 3.4 mL of nitric acid and 10 mL of water was added prior to the measurements. The obtained solutions were then analyzed in a sequential ARL model PerkinElmer 3410 machine.

X-ray diffraction (XRD) experiments were carried out on a Rigaku X-ray diffractometer (Rigaku model, 40 kV and 25 mA) using CuKα radiation. Crystal structures were determined using low-angle ($2\theta = 1–8°$) and wide-angle diffraction patterns in the $2\theta = 3–80°$ range.

Scanning electron micrographs were recorded using a Philips XL-30 (EDX Link Analytical QX-20000 system coupled to the SEM microscope). The fresh and spent samples were deposited on a sample holder with an adhesive carbon foil and sputtered with gold for viewing with a scanning electron microscope.

N_2 adsorption–desorption isotherms were used to examine the porous properties of both fresh and spent samples by using nitrogen as the adsorbent at −196 °C. The measurements were carried out in a Micromeritics ASAP 2002 instrument. Before the analysis, all samples were pretreated in a vacuum at 100 °C for 12 h.

TPR measurements of fresh catalysts were carried out in home-made equipment in the range of 50–1000 °C at a heating rate of 10 °C min^{-1}. A 5% H_2/N_2 mixture was used. Before the analysis, samples of ca. 0.1 g were placed in a quartz tube reactor and heated under nitrogen at 100 °C for 2 h. Thermoprogrammed oxidation experiments for the spent catalysts (TPO) were performed in the same equipment using a mixture of 10% N_2/O_2 and a heating rate of 5 °C min^{-1}, ranging from 25 to 1000 °C.

TGA and DSC experiments for spent catalysts were carried out using Netzsch STA 409 PC/PG equipment coupled to a Bruker Tensor 27 IR instrument. The measurements were performed on spent catalysts to examine the coking degree of the spent samples from room temperature to 1000 °C at 10 °C min^{-1}, under air flow by placing approximately 15 mg of the sample in an aluminum pan.

EPR experiments were performed in order to study the oxidation state of the metals present in the solids. EPR spectra were taken in a Bruker cavity at room temperature on an upgraded Varian spectrometer operating at 100 kHz field modulation and a frequency of 9–11 GHz in the X-band mode. DPPH was used as a standard for *g*-value determinations.

Raman spectra of the selected spent catalysts were obtained on a T64000 Raman spectrometer (JobinYvon triple spectrometer) under ambient conditions. A 514.5 nm Ar laser was used as the exciting source on the sample surface and a power of 20 mW. The measurements were referenced to Si at 521 cm^{-1} with 16 data acquisitions in 120 s. The lens focus was of 100 times.

2.3. Catalytic evaluation

Dehydrogenation of ethylbenzene with carbon dioxide was carried out in a tubular stainless steel reactor where 0.1 g of catalyst was loaded per run. Before the catalytic measurements, the catalysts were activated *in situ* under a nitrogen or carbon dioxide flow from room temperature to 550 °C over the course of 1 h. Thereafter, ethylbenzene (Fluka, 99.99 wt%) was fed through a vaporizer where the nitrogen flow mentioned above was mixed with carbon dioxide (AGA 99.99 wt%, with a molar ratio CO_2/EB = 30). The mixture was then passed through the reactor continuously. The reaction was operated at atmospheric pressure in the range of 530–650 °C. The products of the reaction were condensed in an ice/water trap and analyzed by a gas chromatograph (Simple Chrom model) equipped with a flame ionization detector. The gaseous effluents (CO_2, CO and CH_4) were analyzed in a thermal conductivity gas detector chromatograph (Ciola model).

3. Results and discussion

3.1. XRD and EPR studies

Fig. 1 shows the small- and wide-angle XRD patterns of the MeDM and MeO_x/IM catalysts.

In the range of $2\theta = 1–8°$, Fig. 1a shows that XRD features of all the samples are rather similar, and four well resolved diffraction lines are observed and indexed to the (1 0 0), (1 1 0), (2 0 0) and (2 1 0) reflections. This kind of XRD profile is characteristic of the hexagonal mesostructure of MCM-41 reported earlier [27]. For

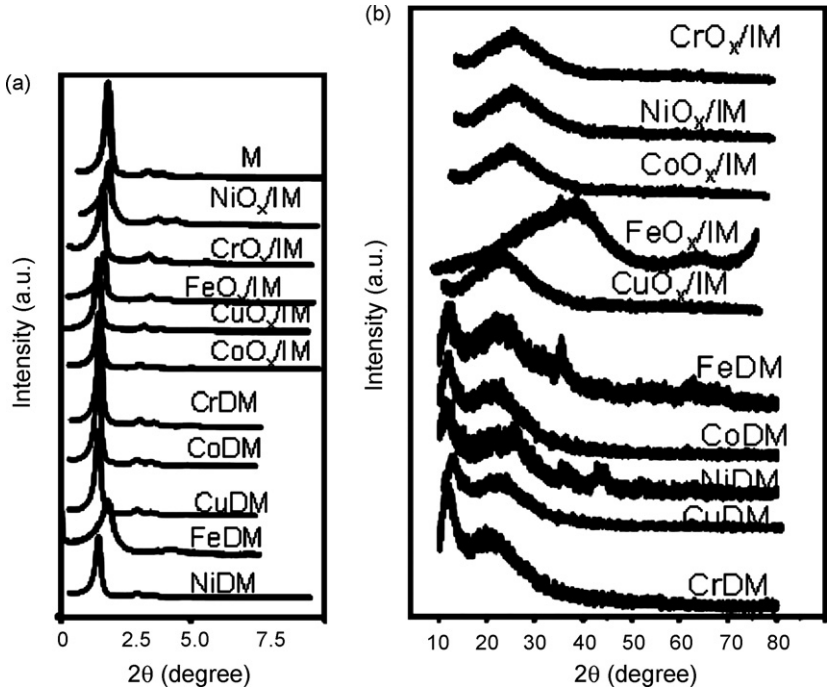

Fig. 1. XRD patterns of calcined MeDM and MeO_x/IM samples: (a) small-angle region and wide-angle region (b).

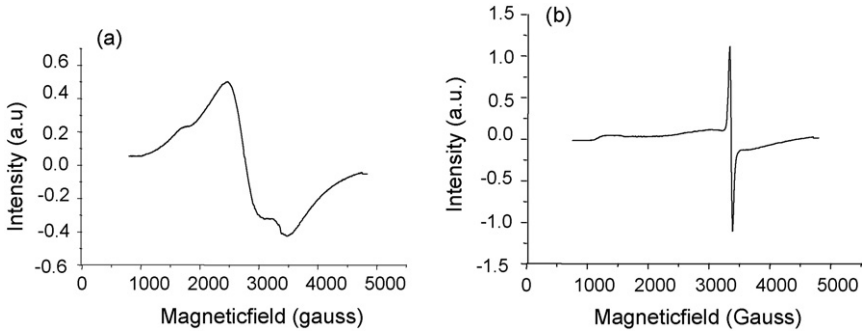

Fig. 2. EPR spectra taken at room temperature of (a) NiDM and (b) NiO_x/IM samples.

NiDM and FeDM, the (2 1 0) lines disappeared without structural disorder of the MCM-41 framework. Indeed, the introduction of Fe or Ni by isomorphous substitution shifts the diffraction peaks to higher 2θ values than the M sample. This fact is associated with the decrease of periodicity over the FeDM and NiDM samples and is in good agreement with previous work [28].

In the case of NiO_x/IM and FeO_x/IM, the gradual decrease in the intensity of the diffraction peaks compared to those of purely siliceous MCM-41 suggests that there is a deterioration of the ordered pore structure. This phenomenon was also observed in other analogous materials [25,29] and was attributed to Ni and Fe providing changes in the coordination spheres of the materials.

The intensity of the diffraction peaks in the small-angle region of the other metal-impregnated samples (IM) was retained, suggesting that there was no deterioration of the ordered structures.

XRD patterns in the wide-angle (Fig. 1b) showed that the catalysts prepared by neither incipient impregnation (MeO_x/IM) nor the isomorphous substitution method (MeDM) had any diffraction lines corresponding to the crystal phase of the Me^{n+} ions or oxides due to the detection limit of the XRD technique as well as the incorporation of these chemical entities into the MCM-41 framework and/or by the high dispersion of the oxides. However, NiDM and Fe-containing catalysts had diffractions peaks corresponding to NiO and Fe_2O_3 oxides, in accordance with the observation of the shift of the diffraction lines at low diffraction angles for these samples.

This is explained by the fact that even at a low content (approximately 1 wt%), the incorporation of metal cations with ionic radii larger than Si^{4+} (0.40 Å) leads to larger M–O bond distances [30]. The ionic radius of Fe^{3+} (0.74 Å) and Ni^{2+} (0.69 Å) is larger than that of Si^{4+}, and thus, the values of a_o of FeDM and NiDM, i.e., 42.8 Å and 42.7 Å, respectively, are close to M, whose value is 42.2 Å, as seen in Table 1. This is an indication of partial incorporation of Fe^{3+} and Ni^{2+} ions into the MCM-41 framework. These metals can also exist in small Me oxide clusters as octahedrallly coordinated NiO and Fe_2O_3 species after calcination [29–31].

Indeed, the amorphous features of XRD of all the IM samples are similar to those of the DM samples in wide-angle (Fig. 1b). The color of the Ni-containing catalyst is black, while that of the Fe-containing catalyst is pale brown after calcination at 550 °C, which indicates the signals of NiO and Fe_2O_3 in these solids, and supports the previous results regarding the elongation of the metal–oxygen bond distance of the MCM-41-based materials [28,30]. The a_o values of the other DM samples are larger than the M value, suggesting an enlargement in the unit cell parameters of the substituted materials after incorporation of metal cations. No clear correlation of the a_o value of the IM samples and their structural features was found.

The EPR technique is a very sensitive tool to obtain information on the chemical environment and the coordination states of metals in mesoporous MCM-41 materials [26,27]. The EPR spectra of the calcined MeDM and MeO_x/IM catalysts displayed typical spectral features of metallosilicates (Fig. 2).

Cr^{3+}, Cu^{2+} and Co^{2+} present calculated free energies of electron (g value) of 1.98, 2.05 and 2.24, respectively, which corresponds to the metals incorporated inside the framework of MCM-41 [25,28], and these are in good agreement with the XRD results. The EPR analysis of the IM series shows g values of 4.2, 2.3 and 3.2, for Cr^{3+}, Cu^{2+} and Co^{2+} species, respectively, and these values are also ascribed to the presence of isolated Me^{n+} ions highly dispersed on the wall surface within the MCM-41 mesopores [31–33]. Interestingly, the signal observed for CuO_x/IM at higher magnetic fields corresponds to a g value of 2.07 while the hyperfine splitting pattern of Cu^{2+} ($I = 3/2$) was observed at lower magnetic fields with a g value of 2.4 that is typically due to CuO particles [31–33]. Indeed, Fe^{3+} and Ni^{2+} prepared by both methods are found to be in isolated oxides that are well-dispersed on the surface of the MCM-41 mesoporous materials, which is in agreement with the reports on these catalysts [33].

Table 1
Properties of MeO_x/IM and MeDM catalysts.

Sample	Metal (wt%)	a_o (Å)	Sg ($m^2\ g^{-1}$)	V_p ($cm^3\ g^{-1}$)	D_p (nm)
M	–	42.2	1108	1.03	3.4
FeDM	0.79	42.8	541	0.76	1.3
CrDM	0.95	43.4	573	0.50	1.6
CuDM	1.06	46.7	587	0.80	1.8
CoDM	0.80	45.3	453	0.64	2.0
NiDM	1.10	42.7	462	0.66	1.7
FeO_x/IM	1.60	42.5	406	0.36	1.3
CrO_x/IM	1.20	44.6	501	0.45	1.6
CoO_x/IM	1.70	43.8	420	0.37	1.3
NiO_x/IM	1.90	43.0	398	0.35	1.2
CuO_x/IM	1.00	42.3	590	0.52	0.9

$a_o = 2d\sqrt{3}$

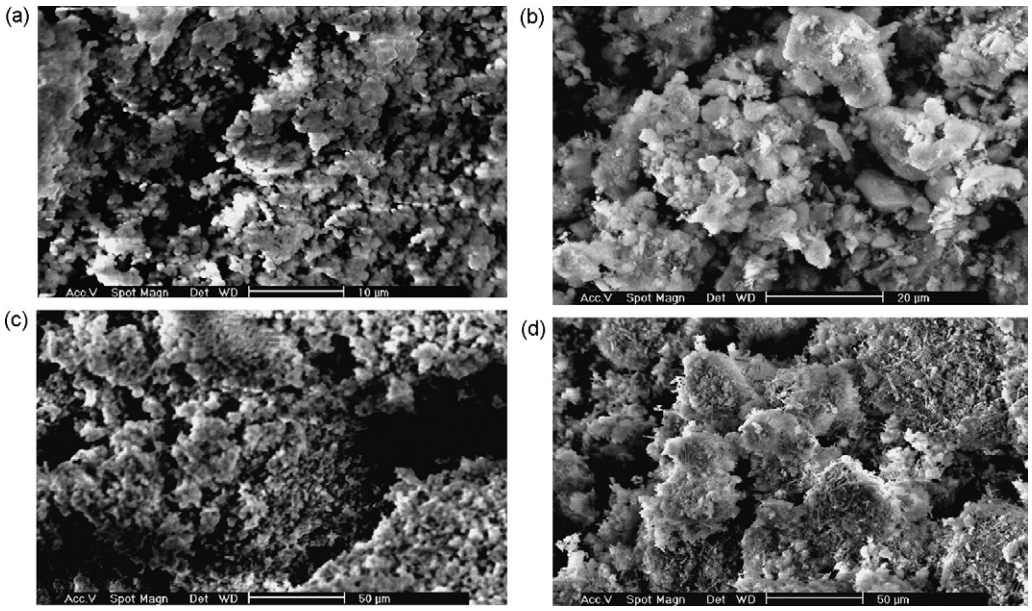

Fig. 3. SEM images of the catalysts studied: (a) M, (b) NiO_x/IM, (c) FeO_x/IM, and (d) CrO_x/IM.

3.2. Chemical analysis and textural features

The metal content was approximately 1 wt% for all MeDM and MeO_x/IM series of solids, and their Si/Me ratio was close to 90 (Table 1).

However, the metal-loaded samples have diminished Si/Me ratios (≅50) in comparison with those of the MeDM series due to the slight increase in the metal content in these solids. At the same Me loading level (Table 1), the catalysts prepared by neither methods exhibit diffraction lines of MeO_x (Fig. 1b), with the exception of the Ni- and Fe-containing samples. This implies that nickel or iron species are mostly dispersed/incorporated on the MCM-41 structure.

N_2 adsorption–desorption isotherms of the MeO_x/IM and MeDM series are of type IV and show steep hysteresis of type H1 at low relative pressure. The sharp inflection observed at pressures ranging from 0.2 to 0.4 suggests that these materials have a regularity of the mesopores structure [25,27].

Table 1 exhibits the textural features of the solids. Purely siliceous MCM-41 has the major values of textural properties: a surface area of 1108 $m^2\,g^{-1}$, a pore volume of 1.03 $cm^3\,g^{-1}$ and a size of 3.4 nm. The incorporation of metals provides a drop in volume and surface area, whereas little change in average pore size was observed in the isomorphous substituted samples when compared with siliceous MCM-41.

The drop in surface area and pore size could be a result of a certain amount of Me incorporation in the MCM-41 structure, which is limited, and the metals can be partially dispersed in the MCM-41 framework or partially dispersed as fine MeO_x oxides on the pore (not detectable by XRD analysis).

The textural features of MeDM samples are rather similar to those of MeO_x/IM. However, as the contents of the metals are slightly higher on the latter, the MeO_x species impose a partial blocking of the pores, mainly in the case of the NiO_x/IM and FeO_x/IM samples. These NiO or Fe_2O_3 entities are deposited onto the MCM-41 surface by manipulating the physicochemical properties of the porous materials. This is confirmed by the small shift to a lower pore diameter upon loading of MeO_x, which is reflected in the formation of particles inside the mesopores of the MeO_x/IM catalysts.

3.3. SEM–EDX analysis

The SEM image of MeDM catalysts shows that they are made up of spherical particles (Fig. 3a) ranging from 1 to 3 nm that are formed during the preparation of the isomorphously substituted samples. Aggregates of such spherical particles are observed for MeO_x/IM catalysts. For instance, NiO_x/IM (Fig. 3b) and the co-presence of irregularly spherical morphology were detected (Fig. 3c).

The SEM micrograph of CrO_x/IM (Fig. 3d) is interesting because it has a high dispersion of small Cr particles deposited on surface of the silica (as suggested by the EDX analysis).

These particles exist in various sizes and are bigger than those of the MeDM series of samples (e.g., 5–10 nm). We propose that such a transformation in particle morphology might be associated with the dispersion of the MeO_x that possesses weaker interaction

Table 2
H_2-TPR results of the catalysts.

Sample	T_{max} (°C)	H_2 consumption (μmol g^{-1})	H_2/Me_{total} (μmol g^{-1})
FeDM	330; 510–700	1070	14.0
CrDM	380; 510	193	2.0
CuDM	350	45	0.45
CoDM	500	201	2.5
NiDM	>850	858	7.8
FeO_x/IM	320; 500	412	2.6
CrO_x/IM	200; 300–510	766	6.3
CoO_x/IM	530	184	1.1
NiO_x/IM	400; 610	517	2.7
CuO_x/IM	300	70	0.7

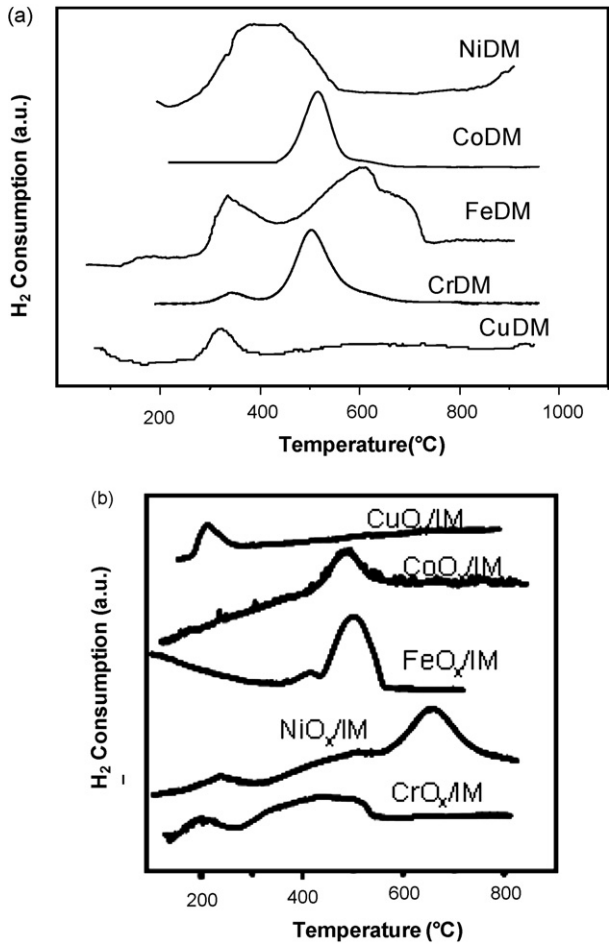

Fig. 4. TPR analyses of solids: (a) MeDM and (b) MeO_x/IM samples.

of metals with the siliceous MCM-41 support. This agrees with the textural properties that showed the changes provided by the low amount of crystalline MeO_x oxides deposited on the mesopores of MeO_x/IM catalysts.

3.4. H_2-TPR profiles

The reduction profiles of the catalysts are comparatively studied to investigate the reducibility of the Me species and their main features are summarized in Fig. 4 and Table 2.

In the case of Cr-containing catalysts, two peaks of approximately 380 °C and 510 °C were observed for CrDM (Fig. 4a), while a peak at 200 °C and a broad peak at 300–510 °C were seen for the CrO_x/DM catalyst. The presence of these two peaks can be ascribed to the reduction of Cr^{6+} to Cr^{3+} or Cr^{2+} species [34]. The easier reduction of CrO_x/IM (Fig. 4b) indicates the existence of Cr_2O_3 interacting weakly with the MCM-41 support, whereas the CrDM catalyst has its Cr ions in the MCM-41 framework, which makes reduction difficult. In addition, CrO_x/IM has the highest H_2/Me ratio among the IM samples (e.g., 6.3 μmol g^{-1}) due to the highest H_2 consumption exhibited by Cr_2O_3 species on the solid surface.

The H_2-TPR profiles of Cu-containing samples show only a reduction peak at about 350 °C [35] that relates to the reduction of Cu^{2+} to Cu^0. Again, the H_2 uptake as well as the temperature of reduction of the CuDM sample (Fig. 4a) was lower than that of the CuO_x/IM supported material (Fig. 4b). It is most likely that this difference is caused by a low pore diameter (ca. 0.9 nm) and unitary cell parameter (42.3 Å) favoring the formation of Cu species on the solid surface of CuO_x/IM. This can be due to the large radius of Cu^{2+} ions (e.g., 0.96 Å) in comparison with those of the other metal-loaded samples. CuO_x species are easily reduced at 300 °C on a solid surface.

For Fe-containing samples, it is clearly seen that the TPR profiles recorded are not similar to each other, either in the positions of the reduction peaks or in their features. For FeDM, the first peak at 330 °C is related to the transformation of Fe^{3+} to Fe^{2+} [16,36]. A broad reduction peak within the range of 510–700 °C in the H_2-TPR patterns is also shown and it displays the high reducibility of iron. These broad peaks, when resolved into two small ones, are attributed to the transformation of Fe_2O_3 to FeO and its reduction to metallic Fe, which is in good agreement with silica-based catalysts [36]. The TPR pattern of FeO_x/IM exhibits two peaks at 320 °C and 500 °C, which are attributed to the aforesaid reduction of Fe^{3+} to Fe^{2+} and of Fe^{2+} to Fe^0, respectively. The H_2/Me ratio obtained for FeDM was higher (14.0 μmol g^{-1}) as compared to those measured for the other samples.

The reduction behavior of Ni-containing samples is characterized by the fact that two steep reductions occur. For NiDM, the H_2-TPR profile is typical of NiO weakly interacting in the framework of the solid (confirmed by EPR results) with one peak of reduction at 430 °C and another one up to 850 °C; this can be related to the difficult reduction of Ni^{2+} species introduced into the silica framework [37,38]. For the NiO_x/IM sample, the low temperature peak (280 °C) is attributed to the NiO in bulk or interacting with the support. The reduction of bulk NiO is up to 500 °C, which is considerably lower than that of 850 °C, arising from the reduction of nickel in the silica environment of the NiDM catalyst. A slight difference in H_2 uptake of these solids is given in Table 2. NiDM surface availability for the reduction of Ni species is increased in comparison with NiO_x/IM (from textural properties); thus, more hydrogen is consumed, whereas the H_2 consumption of NiDM is increased due to the need to reduce Ni^{2+} linked and/or finely dispersed on the surface of MCM-41. The decrease in the H_2/Me ratio of NiO_x/IM (2.7 μmol g^{-1}) in comparison to that of NiDM (7.8 μmol g^{-1}) is due to the formation of NiO (1.9 wt% of Ni), mostly deposited on the surface of the NiO_x/IM sample.

In the case of Co-based systems, CoDM showed less complex interactions, with a sharp peak at 530 °C, which is ascribable to the single complete reduction of cobalt [37]. However, CoO_x/IM is reduced at 500 °C. According to these findings, Co ions start to reduce to metallic clusters consisting of a few atoms and unreduced (Co^{2+}) with partially reduced Co^{1+} ions, which are distributed both in the framework and on the surface of the MCM-41 pores [39]. The H_2/Me ratio decreased from 2.5 to 1.1 μmol g^{-1} because of the Co loading was increased from 0.8 to 1.7 wt% of Co on the Co-containing samples. This can explain the slightly higher reduction of CoDM in comparison with CoO_x/IM.

From these results, it can be pointed out that the MeDM series of catalysts possessing high values of textural parameters is made up of metals in the framework of the MCM-41 that are difficult to reduce, except for the Ni- and Fe-containing samples. In contrast, some dispersed oxides are found in the MeO_x/IM catalyst series that possess less available surfaces and easier reducibility.

3.5. Catalytic activity in the dehydrogenation of ethylbenzene with CO_2

3.5.1. Effect of pretreatment

The preparation method is generally considered to be an important factor for the structure and dispersion of metal catalysts, and these factors commonly influence the catalyst performance in the dehydrogenation of ethylbenzene [1–17].

The catalytic results are summarized in Table 3.

The catalytic performance of Ni-containing MCM-41 pretreated with N_2 is higher than that of the other solids in

the same conditions. For instance, NiDM and NiO_x/IM have activities of 50×10^{-3} mmol g^{-1} h^{-1} and 32.1×10^{-3} mmol g^{-1} h^{-1}, respectively. By contrast, copper-based MCM-41 presents the lowest activity among the solids studied, for example, CuDM and CuO_x/IM have activities of 6.5×10^{-3} mmol g^{-1} h^{-1} and 1.0×10^{-3} mmol g^{-1} h^{-1}, respectively. After this kind of pretreatment, EPR results identified Cu^{2+}, Cu^0, Co^0, Co^{2+} and Cr^{4+}/Cr^{3+} as well as $Ni^{2+}$and Fe^{3+} species.

These results illustrate that the Ni^{2+} active sites can convert ethylbenzene, whereas the Cu^{2+} sites are less effective. Ethylbenzene conversion on Cr- and Co-containing catalysts of both series of solids shows intermediate values of activity among the samples, with the MeDM series being superior to that of MeO_x/IM. The combination of redox and acid–base bi-functionality mechanisms is responsible for the higher activity of Ni-based catalysts, as suggested by similar metal-containing MCM-41 catalysts [20,23]. In the MeDM sample, the Me^{n+} ions are incorporated into the silicate framework, so the structure of the MCM-41 helps convert ethylbenzene to styrene into its walls where the $Ni^{2+}$and Fe^{3+} ions are located.

In contrast, the N_2 atmosphere could remove the oxidized species from the wall of the MCM-41 structure [20]; consequently, the aforementioned species that were detected by EPR migrate from the solid framework to the surface in the form of oxides and/or reduced species. Thus, the activity is only restricted to a few minutes of reaction. It was evident in Co-, Co- and Cr-based catalysts and thus, it can explain the low performance of the CuDM, CoDM and CrDM samples.

Additionally, there is a change in the structure of MCM-41 after dispersing the MeO_x species, which results in the aggregation and a decrease in the structural regularity of the mesopores as seen by the textural parameters. These MeO_x species are easily reduced on the solid surface (TPR analysis). Hence, the MeO_x/IM series loses their efficiency, and consequently the catalytic performance is decreased since there is a reduction in the possible MeO_x active sites weakly linked to MCM-41 surface. The order of activity of these solids is NiDM > FeDM > CrDM > CoDM > CuDM, with the DM series being more active than the MeO_x/IM series. Nevertheless, further studies are necessary to elucidate the catalyst deactivation after 3 h of reaction.

The selectivity for styrene was modest in all Ni-containing catalysts. However, over Fe- and Cr-containing samples, the selectivity for styrene was above 80%. Higher selectivity values for the monomer together with higher conversion was observed with FeDM and CrDM, as found earlier for similar materials [18,24,36], due to the pairs, Cr^{3+}/Cr^{2+} and Fe^{3+}/Fe^{2+}, which are oxidized by CO_2; this gas reacts with H_2 through the RWGS reaction (IV).

$$CO_2 + H_2 \rightarrow CO + H_2O \quad \text{(IV)}$$

Selectivities of Cu- and Co-containing samples reached almost 100% due to the low conversion level reached by using these solids. In the case of Cr-containing samples, the findings report that the CrO_4 tetrahedra are regenerated by the reoxidation of CrO_6 octahedra with CO_2 [23]. Thus, active phases of chromium in the dehydrogenation reaction are believed to be Cr^{4+}/Cr^{3+} species. Even if the TPR results show a high degree of reduction of these species treated previously with N_2 gas, the styrene monomer is likely the main product.

The Fe^{3+} ion is highly selective for styrene, as noticed by the findings [16]. In other words, reverse interconversions of $Fe^{3+} \leftrightarrow Fe^{2+}$ and also $Cr^3 \leftrightarrow Cr^{2+}$ seem to occur although hydrogen and carbon monoxide are present in the reaction media, as reducing agents. The RWGS reaction (IV) proceeds through a coupling of Fe^{3+} to $Fe^{2+,}$ as well as Cr^{3+} to Cr^{2+} by hydrogen:

$$Fe^{3+}\text{–}O + H_2 \rightarrow Fe^{2+} + H_2O \quad \text{(V)}$$

This reaction is irreversible; however, Fe^{2+} to Fe^{3+}conversion by carbon dioxide over FeDM is likely. The same hypothesis is given for CrDM to explain the high selectivity for styrene.

The products formed on Ni-containing catalysts are styrene, benzene and toluene, which are produced by the thermal degradation of ethylbenzene [9–15].

$$C_6H_5CH_2CH_3 \rightarrow C_6H_6 + C_2H_4 \quad \text{(VI)}$$

$$C_6H_5CH{=}CH_2 + 2H_2 \rightarrow C_6H_5CH_3 + CH_4 \quad \text{(VII)}$$

Indeed, the non-identified products could be methane, ethane and polyaromatics. No differences in terms of selectivity between MeDM and MeO_x/IM were observed. Obviously, the enhancement of the catalytic properties can be attributed to the influence of the metals, e.g., Ni and Fe, in converting ethylbenzene.

In the case of catalysts pretreated under a CO_2 atmosphere, the activity is slightly higher than that of those treated with N_2 (Table 4).

For instance, the activity of NiDM was 66.2 mmol g^{-1} h^{-1}, while the same parameter was 50.0 mmol g^{-1} h^{-1} when the catalyst was activated with N_2. Again, both Ni- and Fe-containing catalysts are the most active solids, with activities comparable to that of the literature [18], whereas the copper solids had the lowest catalytic performance. Additionally, the high activity of Ni- and Fe-containing catalysts in the presence of CO_2 is due to the dissociation of the referred gas on the catalyst surface to produce active oxygen lattice species [20,22]. These oxygen species are able to oxidize the H_2 produced in reaction (II) into H_2O through the reverse shift reaction (RWGS, reaction (IV)); thus, it releases the limitation of thermodynamic equilibrium [10,18] to provide a high catalytic activity.

The selectivity behavior of CO_2-pretreated solids was similar to that of N_2-pretreated solids. Indeed, no effect of the preparation method on the selectivity was observed, and the influence of the

Table 3
Activity and selectivities for styrene (S_{St}), toluene (S_T), benzene (S_B) and non-identified products (S_x). Reaction conditions: pretreatment: N_2; catalyst weight: 100 mg; CO_2/EB = 30; 3 h of reaction.

Sample	Activity ($\times 10^3$ mmol g^{-1} h^{-1})	%Selectivity			
		S_{St}	S_B	S_T	S_x
FeDM	32.0	98.2	–	–	1.8
CrDM	15.0	87.4	2.6	5.4	5.2
CuDM	6.5	99.6			0.04
CoDM	7.0	100			
NiDM	50.0	62.0	27.0	4.9	6.1
FeO_x/IM	13.7	100	–	–	–
CrO_x/IM	9.1	94.9	2.8	2.3	–
CoO_x/IM	2.3	99.8	–	–	0.02
NiO_x/IM	32.1	48.0	23.1	4.8	24.6
CuO_x/IM	1.0	99.0	–	–	1.0

Table 4
Activity and selectivities for styrene (S_{St}), toluene (S_T), benzene (S_B) and non-identified products (S_x). Reaction conditions: pretreatment: CO_2; catalyst weight: 100 mg; CO_2/EB = 30; 3 h of reaction.

Sample	Activity ($\times 10^3$ mmol g^{-1} h^{-1})	%Selectivity			
		S_{St}	S_B	S_T	S_x
FeDM	42.6	95.6	1.3	2.8	0.02
CrDM	27.3	93.7	2.2	4.1	–
CuDM	6.9	100	–	–	–
CoDM	8.1	98.9	–	–	1.1
NiDM	66.2	52.8	14.0	21.3	11.9
FeO_x/IM	11.3	99.3	–	–	0.07
CrO_x/IM	14.6	97.5	–	–	2.5
CoO_x/IM	3.7	99.1	0.09	–	–
NiO_x/IM	44.9	35.6	32.1	8.0	24.3
CuO_x/IM	2.6	100	–	–	–

metals was more pronounced. The CO_2 atmosphere activating the catalysts seems to results in an oxidation of Me species, and the metal surface is kept in a high oxidation state, which comes from the reaction. Therefore, the catalysts activated by CO_2 produced Cr^{4+}/Cr^{3+}, Cu^{2+}, Co^{2+}, Fe^{3+} and Ni^{2+} species in both series of solids, according to EPR analysis.

In contrast, the metal species formed on the N_2-activated solids were rather similar to those of the CO_2-activated ones; however, the highest oxidized species provided by CO_2 when combined with the hard reducibility of isomorphously substituted materials (DM) result in more active catalysts, as compared with the impregnated solids (IM). Indeed, it can be said that lattice oxygen in the DM and IM samples was consumed during the dehydrogenation under an N_2 atmosphere to result in the corruption or weakening of the long-range regularity of the hexagonal arrays while the defect formed by the lattice oxygen uptake can be refilled by oxygen from gas-phase CO_2, resulting in no substantial change in the structure under a CO_2 atmosphere, as previously studied in CrMCM-41-based materials [23].

3.5.2. *Effect of temperature on the conversion and styrene selectivity*

The conversion and selectivity of ethylbenzene at different temperatures are depicted in Fig. 5.

The catalytic performance was very poor (less than 2%) over all Cr-, Co- and Cu-containing samples during 6 h of reaction at all temperatures studied; this is due to the reduction of the metal species. Therefore, the catalytic run was performed for NiDM, NiO_x/IM, FeDM and FeO_x/IM.

Taking Fig. 5 result into account, variation of the ethylbenzene dehydrogenation conversion with increasing the temperature

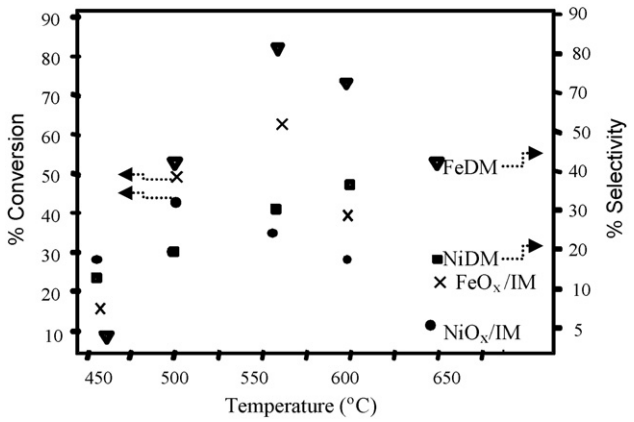

Fig. 5. Effect of the temperature on the conversion and selectivity for NiDM, NiO_x/IM, FeDM and FeO_x/IM. Reaction conditions: 6 h; CO_2/EB = 30; mcat = 100 mg; pretreatment: CO_2.

reveals that the DM solids are more active than the MeO_x dispersed metals (IM). Up to 500 °C, the increase in conversion was linear, reaching about 50% of this catalytic parameter for the Fe-containing samples, while the Ni-containing catalysts had the inverse tendency, reaching almost 36% of conversion at 500 °C, independently of the preparation method. These results indicate that the influence of the M^{n+} or MeO_x species are rather similar, considering that 1 wt% of the referred species are present. The increase in temperature favors M^{n+} leaching from the MCM-41 framework to form MeO_x species; thus, at the final stage, all the active sites of both series of catalysts have the same nature.

The selectivity for styrene over the solids showed a distinct behavior. On one hand, Fe-containing catalysts experienced a slight decrease in selectivity, e.g., 88–70% for FeDM, by increasing the temperature (550–650 °C). Conversely, for Ni-containing catalysts the selectivity was drastically decreased, reaching values close to zero up to 650 °C. In the range of 450–650 °C, both NiDM and NiO_x/IM samples had selectivity values of approximately 40% due to the low conversion achieved for the referred solids after 6 h of reaction.

These results are justified by the fact that an increase in temperature favors the conversion of ethylbenzene due to the endothermic character of the reaction, mainly over Fe^{3+} active sites, which are selective for styrene [2,14]. In contrast, over Ni-containing samples, furnishing energy to the process by means of increasing the temperature initially results in high catalytic performance. As the reaction proceeds, the Ni^{2+} species are reduced in the reaction media to Ni^0 active sites, which are not reoxidized by the CO_2 atmosphere, because they form carbonaceous deposits (further confirmed by Raman spectroscopy), which deactivates the catalysts at relatively high temperatures (>600 °C).

The selectivity for styrene was decreased up to 550 °C due to thermal cracking of ethylbenzene, toluene, benzene, and ethane (reactions (VI) and (VII)). Also, the cracking of ethylbenzene in carbonaceous deposits over Fe-based catalysts cannot be excluded (reaction (VIII)):

$$C_6H_5CH_2CH_3 \rightarrow 8C + 5H_2 \quad \text{(VIII)}$$

In the case of NiDM and NiO_x/IM catalysts, the styrene selectivity is initially high because of the degradation of carbonaceous deposit precursors, i.e., coke precursors, in the presence of water into carbon dioxide and hydrogen [8] on the Ni^0 sites (reaction (IX))

$$\text{cokeprecursors} + H_2O \rightarrow CO_2 + H_2 \quad \text{(IX)}$$

Nevertheless, after 6 h of reaction, the high amount of toluene, benzene and other polyaromatics condensed are deposited on the surface/pores of the Ni-containing samples due to the high amount of Ni^0 species exposed to the reactants. Thus, the selectivity for styrene is drastically decreased.

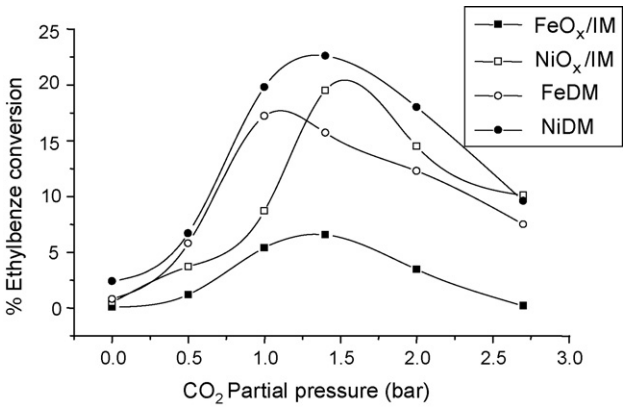

Fig. 6. The partial pressure versus conversion of ethylbenzene for Ni- and Fe-containing catalysts at 550 °C, 1 h; mcat = 100 mg; pretreatment: CO_2.

3.6. Effect of the partial pressure of CO_2 on the conversion of ethylbenzene

The partial pressure of CO_2 was varied by adjusting the molar ratio of CO_2 and N_2, while the ethylbenzene total flow was kept unchanged. The preparation method has almost no influence on the catalytic performance; however, the metal nature has a significant influence. Since CO_2 has a profound influence on the catalytic activity, in the absence of this gas ethylbenzene conversion is low over all catalysts (less than 2.5%), as seen in Fig. 6.

Small amounts of CO_2 ($P_{CO_2} = 0.5$ bar) give an ethylbenzene conversion of approximately 6.0% with the FeDM while FeO_x/IM conversion is modest (less than 2%). Indeed, there is a maximum in terms of conversion for all catalysts studied up to 1.0 bar. An increase in the partial pressure of CO_2 up to 1.5 bar gave a drop in conversion over the FeDM catalyst whereas over the FeO_x/IM catalyst the conversion was not drastically changed. A further increase in the partial pressure of CO_2 results in a decrease in ethylbenzene production because of the low adsorption of ethylbenzene on the catalyst's surface in the presence of an excess of CO_2 [10,22]. The conversion of the Ni-containing catalysts is superior independently of the preparation method.

In all cases, the selectivity for styrene was not been substantially changed over FeDM and FeO_x/IM. However, both NiDM and NiO_x/IM had selectivities lower than 50%, indicating that CO_2 is unable to oxidize Ni^0 species, which is not selective for styrene.

According to the mechanistic considerations of oxidative dehydrogenation of ethylbenzene, H-abstraction of ethylbenzene by a basic surface oxygen located at a defect site has been proposed [41], which would leave two OH groups at the surface. The direct recombinative desorption of hydrogen in the form of water under the consumption of surface oxygen is most likely. At the final step, the reoxidation of Fe^{3+}/Fe^{2+} pairs by dissociative adsorption of CO_2 added to the feed is possible, as observed over iron oxide catalysts.

Therefore, in the case of FeDM catalysts, intermediates of ethylbenzene are dissociated at the α-position of this molecule. Indeed, neutrally adsorbed molecular oxygen species and O^- species of the catalysts demonstrate the ability to activate CO_2 according to deuterium exchange experiments [42]. Thus, the reaction of ethylbenzene with CO_2 has been shown to occur on O^- species [3,14,20]. Since the former species are consumed by the reaction, CO_2 supplies the deficiency of the catalyst, especially on FeDM. Hence, the Fe^{3+} acid site of the catalyst adsorbs ethylbenzene (Fig. 7), reversibly abstracting the α-hydrogen at a basic OH adjacent to the acid site. The base sites, e.g., oxygen species and O^- species, activate the gaseous CO_2 to form an O^- entity, which abstracts the β-hydrogen.

At the same time, the interconversions of $Fe^{2+} \leftrightarrow Fe^{3+}$ can occur when carbon dioxide is present in the reaction. Simultaneously, hydrogen also may reduce the Fe^{3+} acid site in a parallel reaction, mainly on FeO_x/IM, on which deactivation is severe. Finally, the carbon monoxide may react with water or oxygen by generating carbon dioxide:

$$CO + H_2O \rightarrow CO_2 + H_2 \quad (X)$$

$$CO + 0.5O_2 \rightarrow CO_2 \quad (XI)$$

However, there is an optimum level of CO_2; if this circumstance is achieved, the catalysts deactivate because of the RWGS reaction (reaction (IV)), which is further translated to syngas formation; thus, a thermodynamic equilibrium is achieved as observed in mechanistic studies [41,42]. Ni-containing catalysts have styrene selectivity decreased because of deactivation of the nickel sites by coking, which grows on Ni^0 sites.

3.7. Characterization of spent catalysts

The catalysts were exposed to a complex gas environment under reaction conditions, which suggests researching the causes of catalyst deactivation. In order to understand the origin of catalyst deactivation, we have characterized the spent catalysts by TPO,

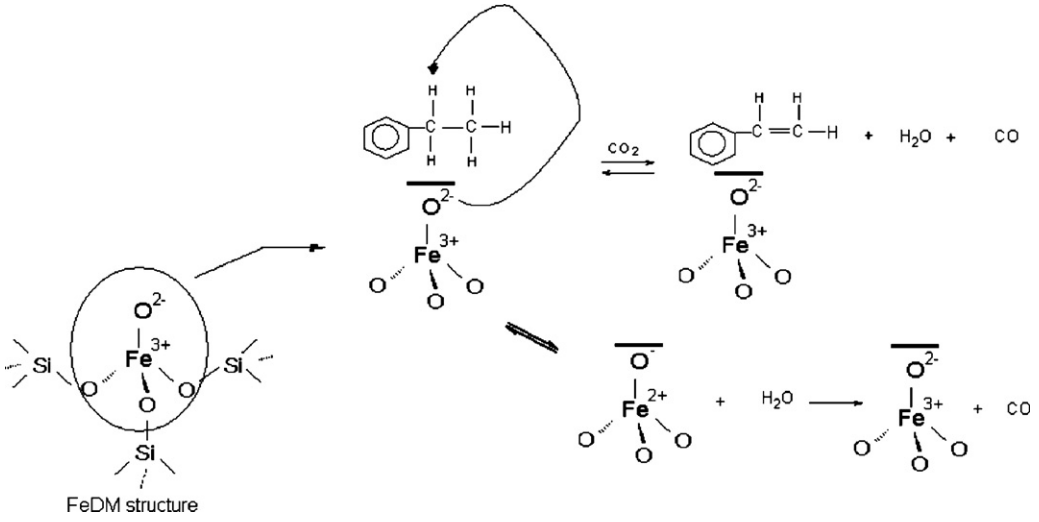

Fig. 7. Schematic representation of the dehydrogenation of ethylbenzene over FeDM catalyst.

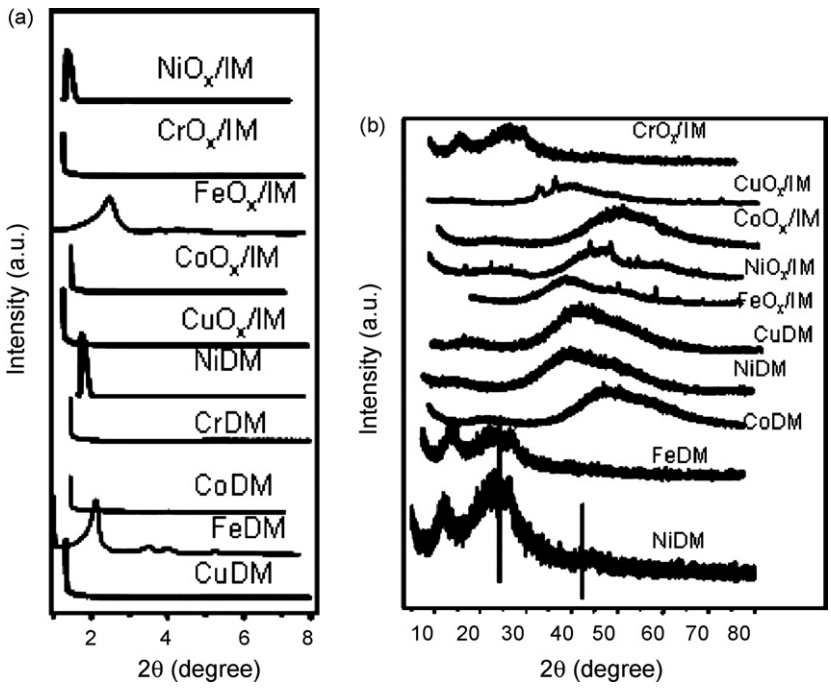

Fig. 8. XRD diffractograms of spent catalysts. Small (a) and wide (b) diffraction angles.

XRD, Raman spectroscopy, textural features, thermal analyses and EPR techniques.

After the reaction, there was a collapse in the MCM-41 structure and/or a decrease in regularity of the hexagonal array in Cu-, Cr- and Co-based catalysts (Fig. 8a), whereas Fe- and Ni-containing catalysts had their structure preserved, according to XRD analysis.

The XRD results from a wide-angle of diffractions (Fig. 8b) indicate that Cu-, Cr- and Co-containing catalysts have peaks that are characteristic of Cu^0, Co^0, and Cr^{3+}/Cr^{2+}, which is in accordance with the *g* values obtained for the spent catalysts by EPR experiments [31,32]. These species were not detected by XRD after the catalytic run due to the limitations of this technique. It suggests the high reducibility of Cu^{2+}, Co^{2+} and Cr^{4+}/Cr^{3+} after their use in ethylbenzene dehydrogenation. On the other hand, Fe- and Ni-containing catalysts have peaks corresponding to NiO and Fe_2O_3, aside from the peaks ascribed to carbon species deposited on the solid surface at $2\theta = 25.3^\circ$ and 42.5° [8]. From these results, it seems that the preparation method does not influence the deactivation of the solids. The nature of the metals present on the MCM-41stucture seems to be more relevant.

Table 5 shows the physicochemical properties of spent catalysts. It can be seen that the surface area and pore diameter values decreased after the catalyst test, by comparing the values presented in Table 1. It was not possible to measure the particle size of both FeO_x/IM and NiO_x/IM samples due to the large amount of coke on the solids surface.

Table 5
Physicochemical properties of spent catalysts.

Sample	Sg ($m^2\ g^{-1}$)	Particle size (nm)	Species identified by EPR
CuDM	328	23.1	Cu^0
FeDM	534	2.8	Fe^{2+}; Fe^{3+}; C
CoDM	240	17.5	Co^{2+}; Co^0
NiDM	456	1.9	Ni^{2+}; Ni^0; C
CrDM	148	10.6	Cr^{2+}
FeO_x/IM	203	–	Fe^{2+}; C
CrO_x/IM	102	38.5	Cr^{2+}
CoO_x/IM	286	20.8	Co^{2+}; Co^0
NiO_x/IM	308	–	Ni^0; C
CuO_x/IM	285	28.0	Cu^{2+}; Cu^0

Specifically, over the CuDM, CrDM and CoDM samples, the values of surface area were slightly higher than those of CuO_x/IM, CrO_x/IM and CoO_x/IM. Also, these results are in line with an increase in the particle size observed after the catalyst test, which suggests a phase transformation. Hence, there was a sintering of these solids, which explains the low performance of these catalysts in the reaction. In contrast, Fe- and Ni-containing samples experienced a decrease of less than 5% in their surface area in comparison with the fresh values of this parameter (Table 1).

3.7.1. Coke analysis

In order to investigate the causes of the deactivation of the Ni- and Fe- containing catalysts, which were deactivated by coking, the content and nature of the carbon species deposited after 24 h of reaction were investigated by Raman and TPO analyses.

Both FeO_x/IM and NiO_x/IM samples were deactivated after 3 h of reaction by clotting of the reaction tube by coking. However, NiDM and FeDM were active during 24 h of reaction. TPO thermograms of NiDM showed three kinds of carbon, which were attributed to aliphatic carbon, polyaromatics and graphitic carbon at 462 °C, 485 °C, and 568 °C, respectively. In contrast, only one kind of carbon was found deposited on the FeDM sample, which was burned off at 450 °C, as seen in Fig. 9. This explains the ease in alleviation of coking by using CO_2 with the FeDM sample.

TG and DSC curves showed that the spent catalysts had a mass gain event in the temperature range 200–400 °C, probably due to the oxidation of the remaining metals present on FeDM and NiDM samples. In addition, both samples had a further mass loss event centred at 500 °C which was attributed to the combustion of amorphous (non-graphitic) carbon, derived from the reaction, mainly on NiDM that had the greatest proportion of non-graphitic carbon. A second mass loss event at approximately 800 °C and 720 °C, respectively for FeDM and NiDM, was observed. This indicates that highly graphitic (or crystalline) carbons are thermally more stable compared to less crystalline or amorphous carbons [8,38]. The crystalline carbon species can occur on the pore mouth and on the outer surface regions of FeDM particle where they may be readily graphitized. Simultaneously, carbon deposition on the surface as well as

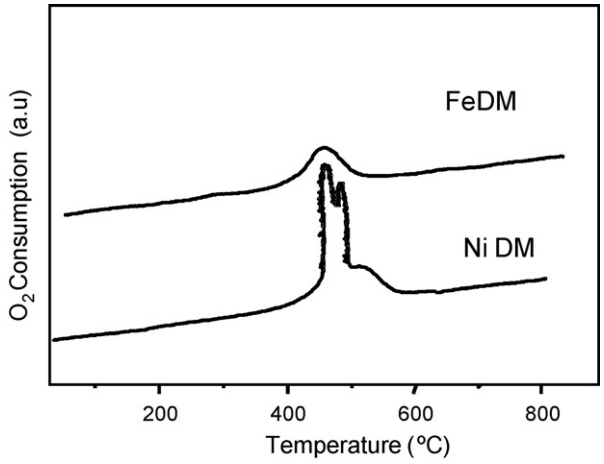

Fig. 9. TPO thermograms of spent NiDM and FeDM samples.

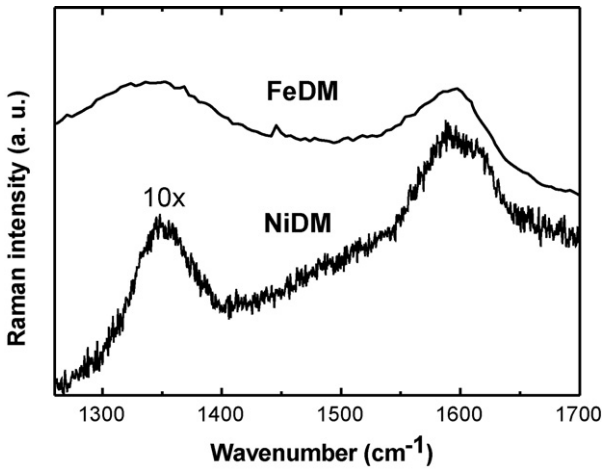

Fig. 11. Raman spectra of spent NiDM and FeDM catalysts.

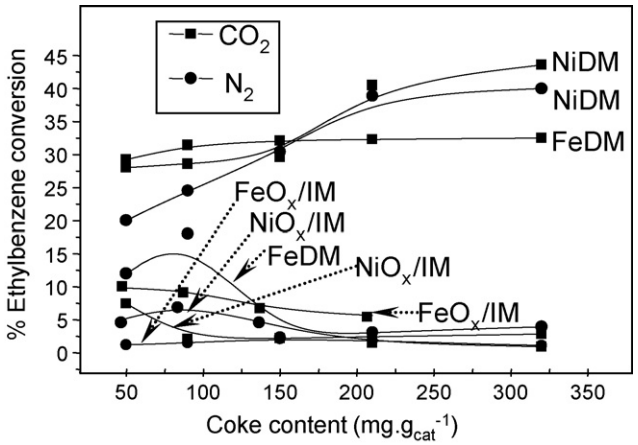

Fig. 10. Coking degree and ethylbenzene conversion under different atmospheres.

within the pores of the mesoporous materials led to amorphous carbon. It can explain the amount of carbon species formed in the dehydrogenation of ethylbenzene with CO_2, which were further confirmed by Raman spectroscopy.

The amount of coke deposited was related to the conversion of ethylbenzene (Fig. 10).

There is a correlation between the coke amount and ethylbenzene conversion in each atmosphere where the reaction was performed. In the presence of CO_2, coke formation was diminished and the carbon deposition was not severe over the FeDM sample. The carbon deposits can be removed from the surface of the catalyst by water and generate carbon monoxide and hydrogen, according to the reaction (XII):

$$\text{coke} + H_2O \rightarrow CO + H_2 \quad \text{(XII)}$$

The CO_2 formed upon reaction (IX) acts to reoxidize Fe^{3+} ions on the surface (Fe_2O_3) and on the structure of MCM-41; thus, it provides the catalytic conversion of ethylbenzene in line with the EPR analysis of spent catalysts that detected Fe^{3+} species. However, over the NiDM sample, the coking was intensified in the presence of N_2 or CO_2 due to the Ni^0 species, which are prone to form carbonaceous deposits [8,38]. In this case, the CO_2 does not behave as an oxidant for Ni^0 species, and the surface of the solid is covered by coke after 24 h of reaction. The nature of the carbon species formed on the solids was investigated by Raman spectroscopy (Fig. 11).

The Raman spectra of the spent NiDM sample shows a strong G band peak at 1590 cm^{-1}, which is ascribed to the graphitic structure of carbon, and a small D band peak around 1349 cm^{-1} corresponding to disordered carbon, such as amorphous carbon.

In the case of FeDM, the band at 1345 cm^{-1} and 1592 cm^{-1} are related to the D and G bands, respectively. Particles of Fe_2O_3 are also observed, as reported in the literature for analogous materials [44,45], whereas the NiDM bands of NiO_x species on carbon-based materials [38,46] were not observed due to the limitation of the equipment.

The Raman spectra show that the ratio between the D band and G band, e.g, I_D/I_G is equal to 0.62 for NiDM while FeDM has I_D/I_G is equal to 0.84, suggesting that the high conversion and low selectivity to styrene over NiDM are related to the degradation of ethylbenzene into carbon species that are highly disordered, i.e., polyaromatics carbon. These species were formed through the

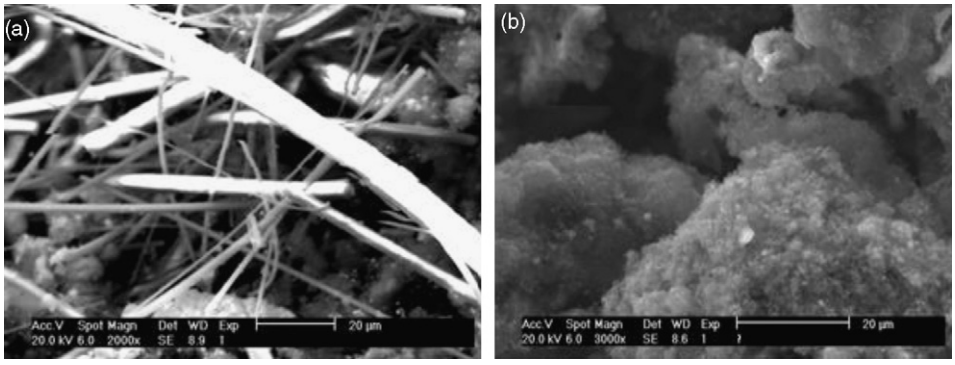

Fig. 12. SEM images of spent catalysts: (a) FeDM and (b) NiDM.

polymerization of styrene and the degradation of other carbon sources (toluene, benzene), the so-called 'quinines, carbon sp^2' or 'active coke' [40,43], which is slightly removed by CO_2.

This clearly indicates that the carbon species are removed in FeO_x/IM and NiO_x/IM samples as the reaction proceeds, so the conversion of ethylbenzene is maintained during 24 h of reaction. On both the NiDM and FeDM catalysts, the coke deposition on the surface of the solids was lower in the presence of CO_2 than in its absence, and this is believed to be the main reason for the deactivation of the catalysts (Fig. 10).

The SEM images of NiDM and FeDM (Fig. 12) show that in the case of FeDM, the structure of this catalyst coexists with carbon filaments; however, these carbonaceous deposits are homogeneous and it covers the surface of the solid, as in the NiDM sample (Fig. 12b).

Over the FeDM catalysts, the coke was totally burned off at 550 °C, making the stable 'sp^2 active species of carbon', which is accessible to CO_2 gas. Consequently, there is an inhibition of the encapsulated carbon present on the Fe^{3+} active sites by the polyaromatics carbon species and the sp^2 active species are burned off by the CO_2. This increases the selective properties of the catalysts due to the continuous Fe^{3+}/Fe^{2+} redox cycle, which is highly selectivity for styrene.

In the case of NiDM, the combustion of coke and the building of new highly disordered polyaromatic species occur on the surface because of the high reactivity of Ni^{2+} and Ni^0 species. As a consequence, the combustion of coke partially occurs due to the new layers of highly disordered polyaromatics (from styrene, benzene and toluene) deposited on the surface, hindering the selectivity of the NiDM catalyst.

From these results, it can be inferred that ethylbenzene dehydrogenation with CO_2 can be done by using MeDM and MeO_x/IM molecular sieves. The Cu^{2+}, Co^{2+} and Cr^{4+}/Cr^{3+}, as well as their oxides, give an initial activity in the reaction; as the reaction proceeds, the referred species are reduced after 3 h of reaction. Nevertheless, Fe^{3+} and Ni^{2+} species are much more active than the other species in the MCM-41 structure. Deactivation studies show that continuous Ni^0 formation enhances the carbonaceous deposition by decreasing the catalyst selectivity, whereas Fe^{3+} species are continuously reoxidized by CO_2, which alleviate coke formation. The Fe^{3+} ions in the structure of MCM-41 result in a highly selective catalyst for styrene production.

4. Conclusions

Based on the above results and discussion, it is concluded that:

(i) Me-incorporated MCM-41 and MeO_x/IM were formed using isomorphous substitution synthesis and the incipient wetness impregnation method, respectively, by producing well-ordered mesoporous-containing metal structures and highly dispersed MeO_x species. Textural and EPR analyses indicated that upon metal incorporation (Cu, Co and Cr), relatively high surface areas were obtained, except for the catalysts with the metals loaded, which had low textural features.

(ii) Cr^{3+}, Co^{2+} and Cu^{2+} species were found as framework species of MCM-41 in the case of isomorphous substituted catalysts or highly dispersed oxides for the impregnated catalysts. However, by both methods of preparation, Fe^{3+} and Ni^{2+} ions were isolated, indicating that Fe_2O_3 and NiO, respectively, exist on the latter solids. The activity of these Co-, Cu- or Cr-containing catalysts in the dehydrogenation of ethylbenzene was restricted to 3 h of reaction due to the high reducibility of the Cr^{3+}, Co^{2+} and Cu^{2+} species compared to that of the Fe^{3+} and Ni^{2+} ions as evidenced by TPR experiments. CO_2 is not able to oxidize these species as seen by EPR.

(iii) Fe^{3+} and Ni^{2+} ions in the structure of MCM-41 are highly active for producing styrene by dehydrogenating ethylbenzene due to both low reducibility and stabilization of these species in the MCM-41 framework. Nevertheless, when the catalysts were impregnated with metals, e.g., Ni and Fe, they demonstrated low performance during the reaction due to the phase transformations of the NiO_x and FeO_x species. Hence, the Me-MCM-41 structure works better to produce styrene regarding M^{n+} stabilization in the MCM-41 framework.

(iv) Deactivation studies show that the coke nature is relevant to the performance of the catalysts. Polyaromatics from styrene on Ni^0 sites rapidly decrease the catalytic selectivity, while 'active sp^2 carbon species' on Fe^{3+} sites are continuously oxidized by CO_2, leading to high catalytic activity. A detailed acid–base and redox mechanism of styrene formation from ethylbenzene on the surface of the catalysts is proposed and is in good agreement with the Fe^{3+} and Ni^{2+} isomorphously substituted catalysts.

Acknowledgments

A.H.M.B. is grateful to the Pibic/Cnpq scholarship. The authors gratefully acknowledged to Dr. M.Y.L.S. for the assistance with EPR analyses.

References

[1] M. Sugino, H. Shimada, T. Turuda, H. Miura, N. Ikenaga, T. Suzuki, Appl. Catal. A: Gen. 121 (1995) 125–137.
[2] N. Mimura, M. Saito, Catal. Today 55 (2000) 173–178.
[3] S. Wang, Z.H. Zhu, Energy Fuels 18 (2004) 1126–1139.
[4] G. Carja, R. Nakamura, T. Aida, H. Niiyama, J. Catal. 218 (2003) 104–110.
[5] T. Badstube, H. Papp, R. Dziembaj, P. Kustrowski, Appl. Catal. A: Gen. 204 (2000) 153–165.
[6] H. Li, Y. Yue, C. Miao, Z. Xie, W. Hua, Z. Gao, Catal. Commun. 8 (2007) 1317–1322.
[7] X.-H. Li, X.W. -Ying, C. Ke, Catal. Lett. 105 (2005) 223–227.
[8] R.M. Freire, A.L. Pinheiro, A.C. Oliveira, F.F. de Sousa, A.P. Ayala, J.M. Filho, P.T.C. Freire, A.C. Oliveira, Appl. Catal. A: Gen. 359 (2009) 165–179.
[9] G.R. Meima, P.G. Menon, Appl. Catal. A: Gen. 212 (2001) 239–245.
[10] D.R. Burri, K.-M. Choi, D.-S.H. Sujandi, N. Jiang, A. Burri, S.-E. Park, Catal. Today 131 (2008) 173–178.
[11] W.D. Mross, Catal. Rev. Sci. Eng. 25 (1983) 591.
[12] I. Serafin, A. Kotarba, M. Grzywa, Z. Sojka, H. Bińczycka, P. Kuśtrowski, J. Catal. 239 (2006) 137–144.
[13] S.-J. Liao, T. Chen, C.-X. Miao, W.-M. Yang, Z.-K. Xie, Q.-L. Chen, Catal. Commun. 9 (2008) 1817–1821.
[14] Y. Sekine, R. Watanabe, M. Matsukata, E. Kikuchi, Catal. Lett. 125 (2008) 215–219.
[15] N. Jiang, D.-S. Han, S.-E. Park, Catal. Today 141 (2009) 344–348.
[16] A.C. Oliveira, J.L.G. Fierro, A. Valentini, P.S.S. Nobre, M.C. Rangel, Catal. Today 85 (2003) 49–57.
[17] F. Cavani, F. Trifirò, Appl. Catal. 133 (1995) 219–239.
[18] Y. Ohishi, T. Kawabata, T. Shishido, K. Takaki, Q. Zhang, Y. Wang, K. Takehira, J. Mol. Catal. A: Chem. 230 (2005) 49–58.
[19] B.S. Liu, G. Rui, R.Z. Chang, C.T. Au, Appl. Catal. A: Gen. 335 (2008) 88–94.
[20] Y. Qiao, C. Miao, Y. Yue, Z. Xie, W. Yang, W. Hua, Z. Gao, Micropor. Mesopor. Mater. 119 (2009) 150–157.
[21] G. Carja, Y. Kameshima, K. Okada, Micropor. Mesopor. Mater. 115 (2008) 541–547.
[22] D.R. Burri, K.M. Choi, J.H. Lee, D.-S. Han, S.-E. Park, Catal. Commun. 8 (2007) 43–48.
[23] K. Takehira, Y. Ohishi, T. Shishido, T. Kawabata, K. Takaki, Q. Zhang, Y. Wang, J. Catal. 224 (2004) 404–416.
[24] D. Wei, N. Yao, G.L. Haller, Stud. Surf. Sci. Catal. 121 (1999) 239.
[25] A.C. Oliveira, N. Essayem, A. Tuel, J.-M. Clacens, Y. Ben Taârit, Stud. Surf. Sci. Catal. 174 (2008) 1239–1242.
[26] M. Grün, K.K. Unger, A. Matsumoto, K. Tsutsumi, Micropor. Mesopor. Mater. 27 (1999) 207–216.
[27] J.S. Beck, J.C. Vartuli, W.J. Roth, M.E. Leonowicz, C.T. Kresge, K.D. Schmitt, C.T.-W. Chu, D.H. Olson, E.E. Sheppard, S.B. McCullen, J.B. Higgins, J.L. Schlenker, J. Am. Chem. Soc. 114 (1992) 10834.
[28] W.A. Carvalho, P.B. Varaldo, M. Wallau, U. Schuchardt, Zeolites 18 (1997) 408–416.
[29] L. Zhang, Y. Zhao, H. Dai, H. He, C.T. Au, Catal. Today 131 (2008) 42–54.
[30] R. Savidha, A. Pandurangan, M. Palanichamy, V. Murugesan, J. Mol. Catal. A: Chem. 211 (2004) 165–177.
[31] C. Mahendiran, P. Sangeetha, P. Vijayan, S.J. Sardhar Basha, K. Shanthi, J. Mol. Catal. A: Chem. 275 (2007) 84–90.

[32] M. Karthika, L.-Y. Lina, H. Bai, Micropor. Mesopor. Mater. 117 (2009) 153–160.
[33] A.V. Kucherov, M. Shelef, J. Catal. 195 (2000) 106–112.
[34] J. Michorzyk, J. Ogonowski, P. Kustrowski, L. Chimierlarz, Appl. Catal. A: Gen. 349 (2008) 62–69.
[35] M.-F. Luo, P. Fang, M. He, Y.-L. Xie, J. Mol. Catal. A. Chem. 239 (2005) 243–248.
[36] J.R.C. Bispo, A.C. Oliveira, M.L.S. Corrêa, J.L.G. Fierro, S.G. Marchetti, M.C. Rangel, Stud. Surf. Sci. Catal. 142 (2002) 517–524.
[37] B.Y. Jibril, S. Ahmed, Catal. Commun. 7 (2006) 990–996.
[38] A.N. Pinheiro, A.C. Oliveira, J.M. Sasaki, A. Valentini, Appl. Catal. A: Gen. 356 (2009) 156–158.
[39] G. Meitzner, G.H. Via, F.W. Lytle, S.C. Fung, J.H. Sinfelt, J. Phys. Chem. 92 (1988) 2925.
[40] G. Emig, H. Hofmann, J. Catal. 84 (1983) 15–26.
[41] M.F.R. Pereira, J.J.M. Orfão, J.L. Figueiredo, Appl. Catal. A: Gen. 196 (2000) 43–54.
[42] A. Schüle, O. Shekhah, W. Ranke, R. Schlögl, G. Kolios, J. Catal. 231 (2005) 172–180.
[43] Z. Li, B.H. Shanks, Appl. Catal. A: Gen. 354 (2009) 50–56.
[44] M. Pérez-Cabero, I. Rodríguez-Ramos, A. Guerrero-Ruíz, J. Catal. 215 (2003) 305–316.
[45] M. Escobar, M.S. Moreno, R.J. Candal, M.C. Marchi, A. Caso, P.I. Polosecki, G.H. Rubiolo, S. Goyanes, Appl. Surf. Sci. 254 (2007) 251–256.
[46] M. Yudasaka, R. Kikuchi, Y. Ohki, S. Yoshimura, Carbon 35 (1997) 195–201.